HAL
open science

Identification of Dynamical Processes at the Tropopause during the Decay of a Cutoff Low Using High-Resolution Airborne Lidar Ozone Measurements

François Ravetta, Gérard Ancellet

▶ **To cite this version:**

François Ravetta, Gérard Ancellet. Identification of Dynamical Processes at the Tropopause during the Decay of a Cutoff Low Using High-Resolution Airborne Lidar Ozone Measurements. Monthly Weather Review, 2000, 128 (9), pp.3252 - 3267. 10.1175/1520-0493(2000)1282.0.CO;2 . insu-01411563

HAL Id: insu-01411563

https://insu.hal.science/insu-01411563

Submitted on 24 Jan 2021

HAL is a multi-disciplinary open access archive for the deposit and dissemination of scientific research documents, whether they are published or not. The documents may come from teaching and research institutions in France or abroad, or from public or private research centers.

L'archive ouverte pluridisciplinaire **HAL**, est destinée au dépôt et à la diffusion de documents scientifiques de niveau recherche, publiés ou non, émanant des établissements d'enseignement et de recherche français ou étrangers, des laboratoires publics ou privés.

Identification of Dynamical Processes at the Tropopause during the Decay of a Cutoff Low Using High-Resolution Airborne Lidar Ozone Measurements

F. RAVETTA* AND G. ANCELLET

Service d'Aéronomie du CNRS, Paris, France

(Manuscript received 2 June 1999, in final form 14 February 2000)

ABSTRACT

In June 1996, an airborne ozone lidar was successfully used to observe the decay of a cutoff low over southern Europe. This weather system was tracked during several days and sampled with an 8-km horizontal resolution. Most of the measurements took place in the 4–12-km altitude range and ozone-rich layers with a vertical thickness often less than 500 m were seen. Ozone vertical cross sections were obtained at the edges of the cutoff low or in frontal regions next to it. Using complementary data it is shown that these bidimensional cross sections characterize the ozone spatial field well. Two main features of the ozone distribution are large variability of the ozone tropopause and the presence of numerous ozone-rich layers within the troposphere. This paper focuses on the first feature. Observed ozone tropopauses compare well with potential vorticity ones derived from ECMWF analyses. The magnitude of the ozone to potential vorticity ratio also indicates that no significant diabatic mechanism contributes to the ozone transfer from the stratosphere to the troposphere above 325 K. An analysis of the evolution of the ozone vertical gradient in the upper troposphere (80–120 ppb) and lowermost stratosphere (120–200 ppb) is used to illustrate its usefulness as a diagnostic tool of dynamical processes. Large differences are found between air masses near and within the cutoff low. Vertical stretching induced by the PV anomaly cannot completely account for them. Differential advection in frontal regions and convective erosion on the eastern edge of the cutoff low tend to sharpen the vertical ozone gradient. On the contrary, clear sky turbulent mixing tends to smooth it. Convective erosion is also likely to transfer ozone from the stratosphere to the troposphere. This is corroborated by ozone vertical cross sections sampling tropospheric air masses three days after the decay of the cutoff low.

1. Introduction

The chemical, dynamical, and radiative balance of the atmosphere is extremely sensitive to the chemical composition of the 8–15-km atmospheric layer. Therefore, perturbations due to human activities must be carefully studied in this altitude range. The upper part of this atmospheric layer, the lower stratosphere, is a strong ozone source to the upper troposphere. The lower part of this atmospheric layer, the upper troposphere, is the main source region to the stratosphere for gases involved in ozone chemical destruction and in stratospheric water vapor budget.

The classical view of the Brewer circulation assumes transport to the stratosphere across the tropical tropopause through convection followed by poleward mean transport circulation and transport to the troposphere at midlatitudes by a combination of diabatic subsidence in the stratosphere and frontgenesis in the troposphere (Holton et al. 1995). In order to better understand this global-scale circulation, intrusions of stratospheric air into the midtroposphere resulting from instabilities of the polar front must be well characterized to quantify the tropospheric ozone budget and the atmospheric's oxidizing capacity over Europe (Kley et al. 1997). Quasi-isentropic deformations of the midlatitude tropopause are very common but may not significantly contribute to chemical tracer exchanges. These intrusions must be stretched to small-scale features in order to achieve an efficient irreversible mixing (Appenzeller and Davies 1992). Instabilities in the jet streams on an isentropic surface may lead to long streamers extending over several thousands of kilometers coupling the subtropical region and the midlatitudes (Langford and Reid 1998). Breakup of these long streamers occurs at intermediate scales between synoptic-scale (>1000 km) and small-scale features (<100 km) where turbulence and radiative processes can mix stratospheric and tropospheric air.

Experimental investigations of air parcels at these intermediate scales are still necessary in order to validate

* Current affiliation: Harvard University, Cambridge, Massachusetts.

Corresponding author address: Dr. Francois Ravetta, Department of Earth and Planetary Sciences, Harvard University, Pierce Hall 109, 29 Oxford Street, Cambridge, MA 02138.
E-mail: fra@io.harvard.edu

© 2000 American Meteorological Society

+3,650/351-,5/.8(4734,./. !"#"! $%##&)+*

modeling work (Lamarque and Hess 1994). Such a study is developed in this paper. We present a field experiment designed to investigate the decay of a cutoff low (COL) and its impact at the tropopause on the transport of chemical species like ozone and water vapor. Such experimental studies in a COL were done in the past using aircraft, satellite, or ground-based observations. Bamber et al. (1984) showed from vertical distributions of long-lived trace gases, ozone, and light hydrocarbons that transport and mixing probably exist in a COL system without specifying mechanisms responsible for such transport. To better understand these mechanisms, Price and Vaughan (1993) followed the time evolution of ozone in a COL using satellite observations, but limited vertical resolution of these data and difficulty accounting for the effect of clouds made interpretation difficult. More recently, ground-based lidar observations with good vertical and time resolution revealed strong variability of the tropopause barrier in such events (Ancellet et al. 1994; Langford et al. 1996). Contrary to Price and Vaughan (1993), however, time evolution could not be properly studied. Here ozone distribution again will be the primary parameter to describe COL evolution.

In order to track the COL area over several days, ozone was measured by an airborne lidar during this experiment. Of course, the ozone distribution reconstructed from the lidar cross sections remains limited because of our inability to forecast precisely enough the motion of the COL and because the lidar instrument cannot provide reliable measurements in clouds. Use of data assimilation techniques combining meteorological analysis and lidar data is probably the only way to obtain an ozone field suitable for numerical models. However use of the airborne lidar remains a definite improvement in the sampling strategy as compared to ground-based stations. This instrument and data processing are discussed in section 2. In section 3, the meteorological situation relative to the campaign is described. In sections 4 and 5, ozone datasets are first presented and are then used to document mechanisms responsible for stratosphere–troposphere ozone exchange. In this paper we will focus on identification of dynamical processes at the tropopause from aircraft datasets and on formulation of questions to be answered by modeling studies. Comparison of ozone data with modeling results will be addressed in another paper.

2. The airborne ozone lidar

a. Description of the instrument

An airborne lidar for tropospheric ozone (ALTO) measurement has been developed to describe the ozone vertical cross section with good horizontal and vertical resolution (Ancellet and Ravetta 1998). This differential absorption lidar (DIAL) system was installed in a Fokker 27 (F27) aircraft to achieve better temporal continuity for analysis of moving meteorological systems. A Nd-YAG laser is used in combination with a single Raman cell to generate three wavelengths that are simultaneously transmitted to the atmosphere: 266–289–316 nm. A 40-cm telescope is used to collect the backscattered light and to focus received photons on a fused silica optical fiber. The sounding angle is 24° off-vertical for the upward-looking configuration when the system is mounted on the F27 aircraft.

The radiation at the exit of the fiber is input into a grating spectrometer for wavelength separation and background sky light filtering. Output of six photomultiplier tubes is recorded by photocounting units and waveform recorders. Combination of two different detection methods provides a dynamical range larger than 7 km for the lidar measurement. Hardware averaging of the waveform recorder and counter outputs has been implemented to allow time for further data processing by the computer. The number of averaged shots can be selected by the operator and is typically 600, that is, a 30-s sampling for an ozone profile. A real-time analysis of the signals is performed to produce a cross section of the ozone concentrations along the flight track. Aircraft data (position, meteorological parameters, ozone measurement by a UV photometer) are recorded every second on a separate tape, and the computer clock is controlled by the aircraft data acquisition system.

b. Data processing

For this campaign, 600-shot averages are further added to increase the signal-to-noise ratio. The maximum number of shots averaged does not exceed 2000, corresponding to horizontal averaging of data over 8 km when using the F27 aircraft. Range averaging of the range-corrected lidar signal is performed with a numerical low-pass filter to improve the signal-to-noise ratio further. The corresponding range resolution is then 300 m at 1 km and 1000 m at 6 km. Of course large ozone structures at smaller scales (100 m) remain visible after this filtering since the sampling is less than 40 m. Correction of molecular extinction (Rayleigh extinction) is based on an atmospheric density model, which depends on season and latitude (Chedin et al. 1985). Analog and photocounting slope signals are combined and ozone concentrations are calculated for two wavelength pairs: 266–289 nm and 289–316 nm. Ozone absorption cross sections are calculated for the three wavelengths using the work of Molina and Molina (1986) including cross-section temperature dependence.

The 266–289-nm wavelength pair is less sensitive to systematic errors (beam alignment, aerosol interferences), but it can only be used for ranges less than 1.8 km since the 266-nm signal is rapidly absorbed in the atmosphere. For ranges above 1.8 km, the pair 289–316 nm is used, except when large aerosol interferences are observed. Indeed, large ozone error is generally associated with these interferences for this wavelength pair.

+3,6!0/3!1-,!/.8(473!4,./. !"#"! $%##&)+*

Although ozone molecular density is the parameter measured by the lidar, the ozone mixing ratio will be used in this paper. The mixing ratio is calculated from ozone molecular density using the atmospheric molecular density model considered for Rayleigh scattering calculations. This may create a 5% bias in the ozone mixing ratio for an unusual temperature profile (i.e., with a 10-K departure from average temperature). Use of meteorological radio sounding data could improve the mixing ratio calculation but this is not necessary for the discussion developed in this paper.

c. *Error analysis*

When no significant aerosol layers are present, the DIAL measurements are limited first by statistical errors related to decreasing signal-to-noise ratios at long ranges and second by systematic errors arising from instrumental limitations, namely geometrical error at near range and electronic noise in the analog signal. No ozone data are calculated when the statistical error becomes larger then 30%. At near range below 1 km, the DIAL measurement remains subject to a bias related to differences between the geometrical telescope overlap function of each emitted laser beam. The shortest distance where an ozone measurement is possible is 500 m, since a 12-ppb overestimate of ozone may exist at shorter ranges. At 750 m, maximum uncertainty associated with the geometrical overlap becomes less than 3 ppb. Residual noise at frequencies less than 50 kHz is frequently apparent in the analog signals and is not always suppressed by averaging. The analog signal at 289 nm becomes noisy above a 2.5-km range, and one must switch to the photocounting signal, which is generally no longer saturated at this range. The narrow overlap range for this wavelength is sometimes a source of error in the ozone calculation at 2.5 km. This can be controlled by a careful examination of the lidar signal slope at this wavelength.

When aerosol layers are present, the aerosol backscatter coefficient is calculated with the lidar signal at 316 nm, where ozone absorption is negligible, using a backward integration scheme described by Browell et al. (1985). This information is used to verify whether significant aerosol layers are present in the measurement area. Cloud layers are then clearly identified and ozone data are removed from these areas because no useful corrections can be made in such conditions. Otherwise, comparisons of the lidar data with other instruments have shown that its accuracy is usually better than 10%–15% (Ancellet and Ravetta 1998).

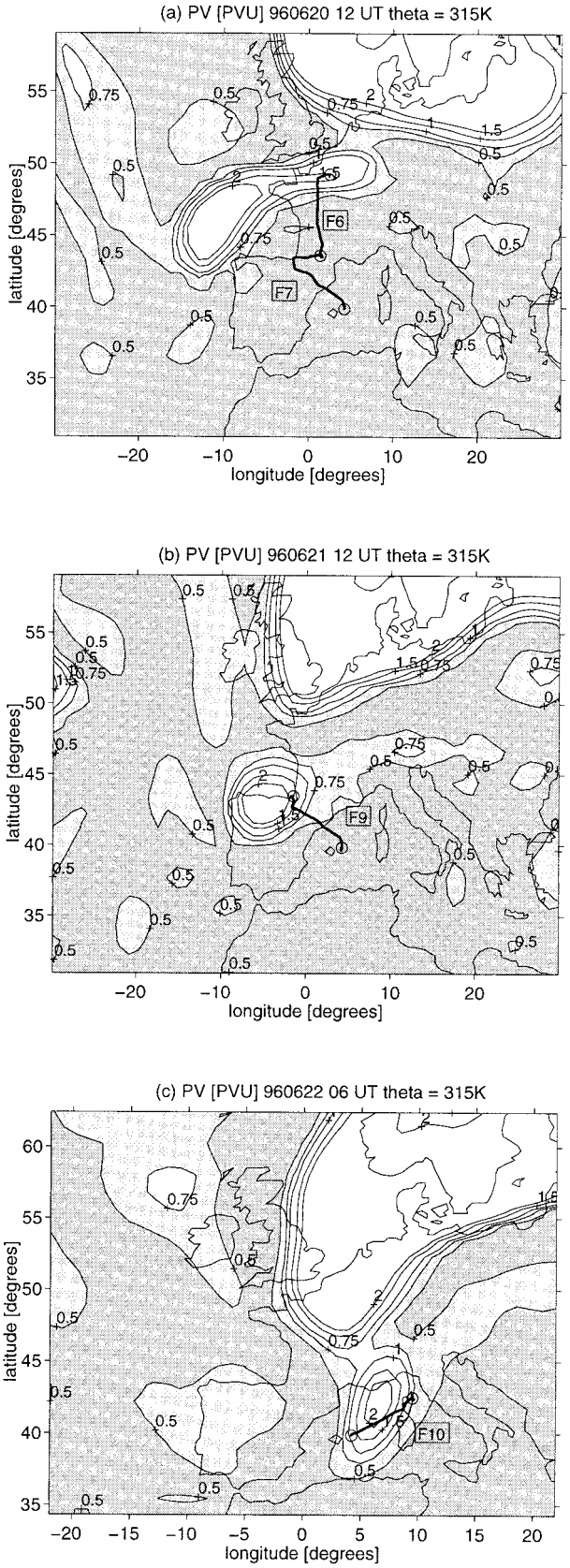

→

FIG. 1. (a)–(c) PV maps at 315 K from 20 to 22 Jun 1996 and (d)–(g) from 23 to 26 Jun 1996. The white areas correspond to PV > 1 PVU. The full black lines are aircraft trajectories. Flight numbers are in boxes (see also Table 1).

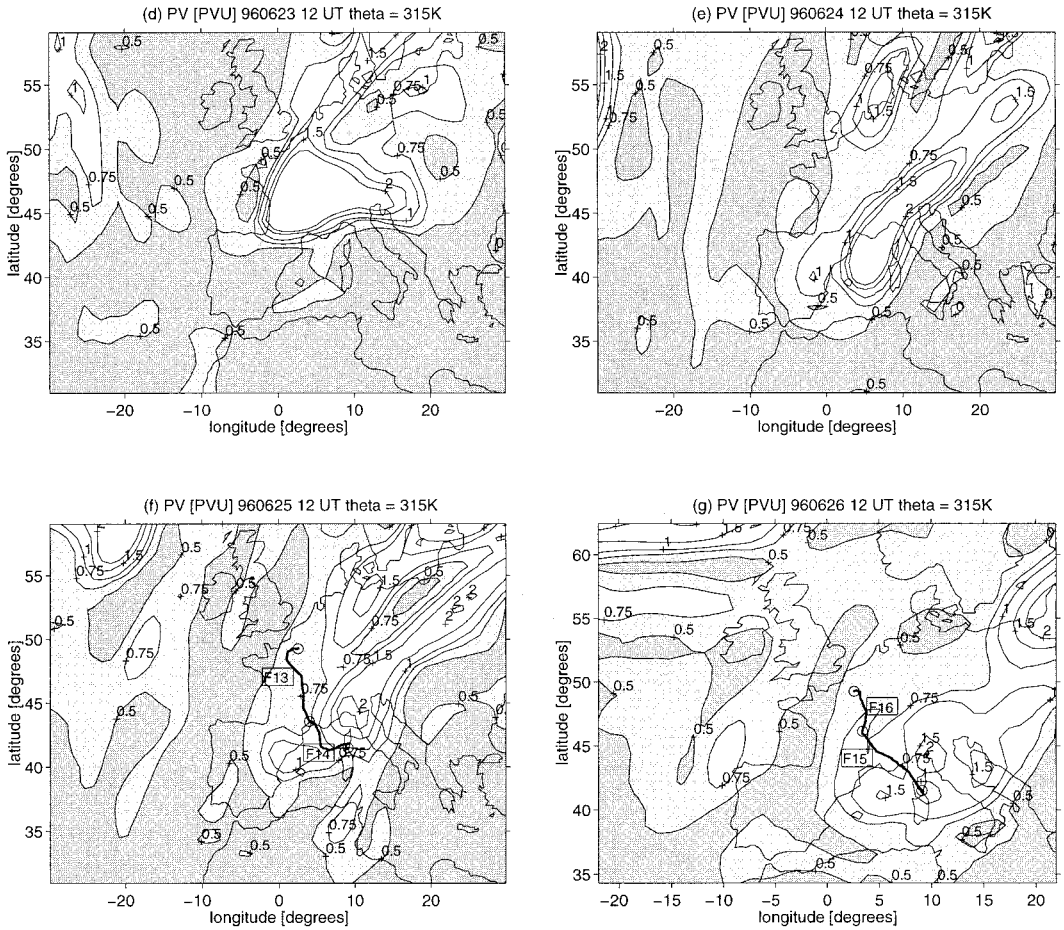

FIG. 1. (*Continued*)

3. Description of the meteorological situation

A cutoff low that forms over the mid–Atlantic Ocean on 14–15 June 1996 drifts eastward over Europe. The potential vorticity field on the 315-K isentropic surface provides a good description of the evolution of the COL. The potential vorticity (PV) was calculated using European Centre for Medium-Range Weather Forecasts (ECMWF) T-106 analyses. On 20 June the COL is located south of England and is stretched over northern France because of a strong zonal flow associated with a well-developed trough over Scandinavia (Fig. 1). According to the IR Meteosat image at 1800 UTC (Fig. 2a), convective clouds over the Pyrénées Mountains are associated with southerly flow on the eastern edge of the COL. Within the COL itself, although cloudiness is also related to convective motion, stratified clouds on the western part of Spain also contribute to the IR radiances seen by Meteosat. This will be verified by the lidar observations.

On 21 June, the COL moves to northern Spain as the trough located over Scandinavia develops over England. The area with PV $>$ 2 PVU (1 PVU $= 10^{-6}$ K kg^{-1} m^2 s^{-1}) decays significantly on this day. The Meteosat image indicates that convection is now present over a significant area within the COL probably because of upslope motions in the Pyrénées Mountains and the Spanish plateau (Fig. 2b). Following the work of Wirth (1995), convection may thus be responsible for the PV diabatic erosion below the tropopause on this day. In the frontal zone south of the COL, a band of cirrus clouds is still clearly visible. These bands of high-altitude stratified clouds on the edge of a PV anomaly are important since they reveal horizontal structures in the humidity field and possibly in the ozone distribution. These layers with different humidity and ozone concentrations may then undergo a strong deformation by differential advection leading to irreversible exchange of air. On 22 June the COL moves rapidly from Spain to Corsica and convection is mainly present on the eastern edge of the COL (not shown).

On 23 June, the COL merges into a large trough that extends southward from the North Sea (Fig. 1) and a new COL was generated. It remains over southern France for three days before dissipating farther to the east. The COL structure during the second phase of this event (25–26 June) is not as well defined. An area of

+3,6:0/3:1-,5/.8(4732:4,./. !"#"! $%##&)+*

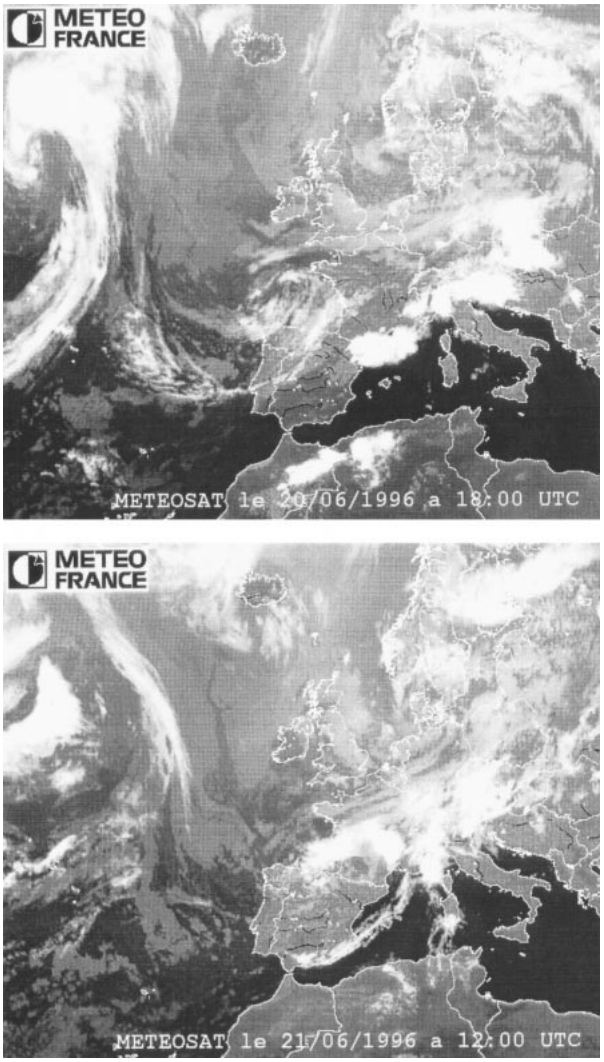

FIG. 2. Meteosat satellite IR image at (a) 1800 UTC 20 Jun and (b) 1200 UTC 21 Jun.

relative PV minimum appears on the edge of the COL since instabilities in the balanced flow over southern France will lead to wave propagation along the PV band (Appenzeller et al. 1996). Existence of these PV deformations at scales smaller than 200 km is important since they lead to new vortices and to fragmentation of the PV anomaly.

4. Ozone measurements relative to the 20–22 June COL

a. *Aircraft data*

1) AIR MASSES SAMPLED BY THE AIRCRAFT

From 20 to 22 June, four aircraft flights were passed near the COL. The flight tracks (Table 1) are indicated by thick black lines in Fig. 1. It was not possible to obtain several cross sections through the COL during its evolution. During flight 10, only, on 22 June, the aircraft sampled several regions within the COL. Flights 6, 7, and 9 are mainly representative of the frontal region around the COL. The wind field at 250 hPa near the tropopause shows that on 20 June, during flight 6 from Paris to Toulouse, the lidar cross section is mainly representative of a transverse cross section through a jet streak (wind > 40 m s^{-1}) in southwesterly flow at the eastern side of the COL (Fig. 3a). At the beginning of this flight the measurements were made near the edge of the COL (Fig. 1). Flight 7, close to 1700 UTC on the same day, was between Toulouse and Minorca Island. During the first part of this flight the aircraft trajectory exhibits a V shape corresponding to a folded vertical cross section through the edge of the jet streak at the eastern side of the COL. Wind values in the jet streak are weaker than before but remain close to 40 m s^{-1} at the westernmost point of the aircraft trajectory. In the second part of this flight, the aircraft flew in a high pressure system with weaker wind speed ($<$20 m s^{-1}) (Fig. 3b). On 21 June the aircraft flew back toward the COL position and the lidar cross section associated with flight 9 is representative first of a cross section at the edge of the COL (Fig. 1) and then of a cross section through the southwesterly flow (Fig. 3c). Thus, these four lidar cross sections obtained near the COL during a 3-day period provide measurements in air masses at different positions from the COL center. Price and Vaughan (1993) showed that different transport mechanisms should act on the ozone profiles around the COL (strong differential advection, convection, turbulent mixing, etc.). Our goal is to identify the signature of these processes in the observed ozone field near the tropopause. Ozone is not a perfect tracer of transport processes from the stratosphere to the troposphere. Recent airborne measurements in frontal systems showed that it can be transported from the boundary layer to

TABLE 1. Aircraft flight times.

No.	Date	Departure	Arrival
F6	20 Jun	Creil (49.3°N, 2.6°E; 1212 UTC)	Toulouse (43.6°N, 1.4°E; 1436 UTC)
F7	20 Jun	Toulouse (43.6°N, 1.4°E; 1524 UTC)	Minorca (39.9°N, 4.2°E; 1812 UTC)
F9	21 Jun	Biarritz (43.5°N, 1.6°W; 1306 UTC)	Minorca (39.9°N, 4.2°E; 1512 UTC)
F10	22 Jun	Minorca (39.9°N, 4.2°E; 0700 UTC)	Bastia (42.5°N, 9.5°E; 0830 UTC)
F13	25 Jun	Creil (49.3°N, 2.6°E; 0818 UTC)	Montpellier (43.6°N, 4.0°E; 1018 UTC)
F14	25 Jun	Montpellier (43.6°N, 4.0°E; 1230 UTC)	Figari (41.5°N, 9.1°E; 1430 UTC)
F15	26 Jun	Figari (41.5°N, 9.1°E; 0842 UTC)	Vichy (46.2°N, 3.4°E; 1106 UTC)
F16	26 Jun	Vichy (46.2°N, 3.4°E; 1324 UTC)	Creil (49.3°N, 2.6°E; 1448 UTC)

+3,650/351-,5/.8(4734,./. !"#"! $%##&)+*

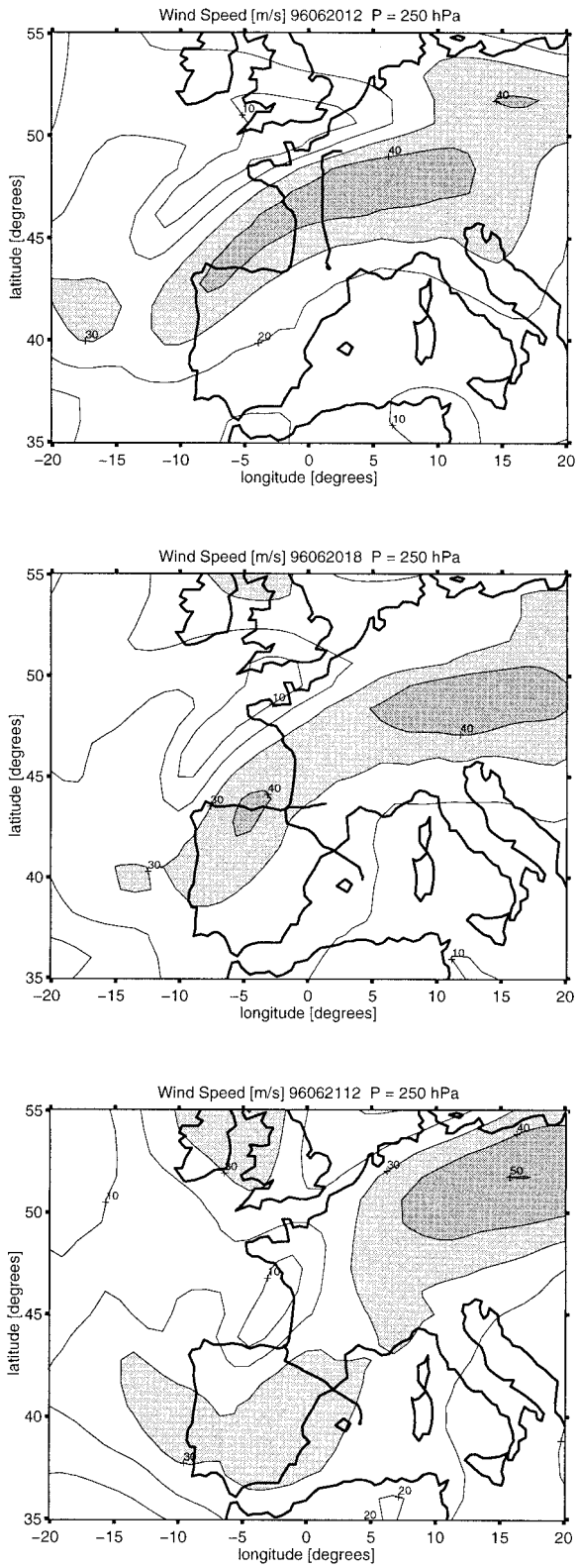

FIG. 3. Wind isotachs in m s^{-1} at 250 hPa at 1200 and 1800 UTC 20 Jun and 1200 UTC 21 Jun. The shaded areas correspond to winds >30 m s^{-1}. The wind is southeasterly in the shaded area. The COL corresponds to wind values less than 10 m s^{-1}.

the upper troposphere (Bethan et al. 1998). However, spring ozone concentrations associated with these events do not exceed 50 ppb in the mid- and upper troposphere, while ozone concentrations, considered in this paper for the discussion of dynamical processes, are in the range 80–200 ppb.

2) OZONE DATASET

The ozone vertical cross sections are presented in Fig. 4 using isomixing ratio contours from 40 to 190 ppb. The contour line step is 10 ppb in the troposphere (40–80 ppb) and increases to 30 and 40 ppb in the tropopause region (80–190 ppb). The color in the area between two contour lines corresponds to the smallest contour value. The 1-h timescale given in Fig. 4 corresponds approximately to a distance of 300 km. The regions with missing data delineate air masses where clouds have been observed. A full strip of missing data is often indicative of convective clouds while missing data above 6 km are associated with altostratus or cirrus clouds. The horizontal distribution of these cloud layers can be derived from Meteosat images (Fig. 2). A UV absorption ozone monitor was mounted in the aircraft for this campaign. These ozone measurements have been included in the lidar cross sections to give the order of magnitude of ozone in the lower and midtroposphere for this meteorological event. Although a direct comparison between the two datasets is not possible, ozone variability in the lowest lidar altitude range compares well with ozone values provided by the ozone monitor. Most of the time, the ozone mixing ratio remains near 60 ppb at altitudes below 5 km suggesting a small impact of photochemical ozone production on the observed ozone distribution and variability in the lower troposphere. Indeed, ozone mixing ratios larger than 80 ppb were measured at 5 km only in the jet streak region at the eastern side with a connection to layers reaching the tropopause (see below).

In Fig. 4, the ozone vertical cross sections exhibit two main features: a variability in the vertical gradient at the tropopause and the occurrence of many ozone layers in the frontal zone around the COL. The ozone vertical gradient appears to be less defined in the return flow at the eastern side of the COL than in the northerly jet on the western side. This is due to larger ozone concentrations below the tropopause in the return flow and it can be interpreted as the effect of stratosphere–troposphere exchange in these air masses. This point will be further developed in section 4b. One could argue that the positive ozone gradient in the upper troposphere is related to ozone photochemical production. But this is very unlikely for this event due to the low ozone concentration in the lower layers. Furthermore, a high-resolution global model study recently showed that, in the upper troposphere, the stratospheric source of ozone increases with altitude, from 20 ppb at 5 km up to 80 ppb at the tropopause, while its photochemical source de-

+3,650/351-,5/.8(4732 4,./. !"#"! $%##&)+*

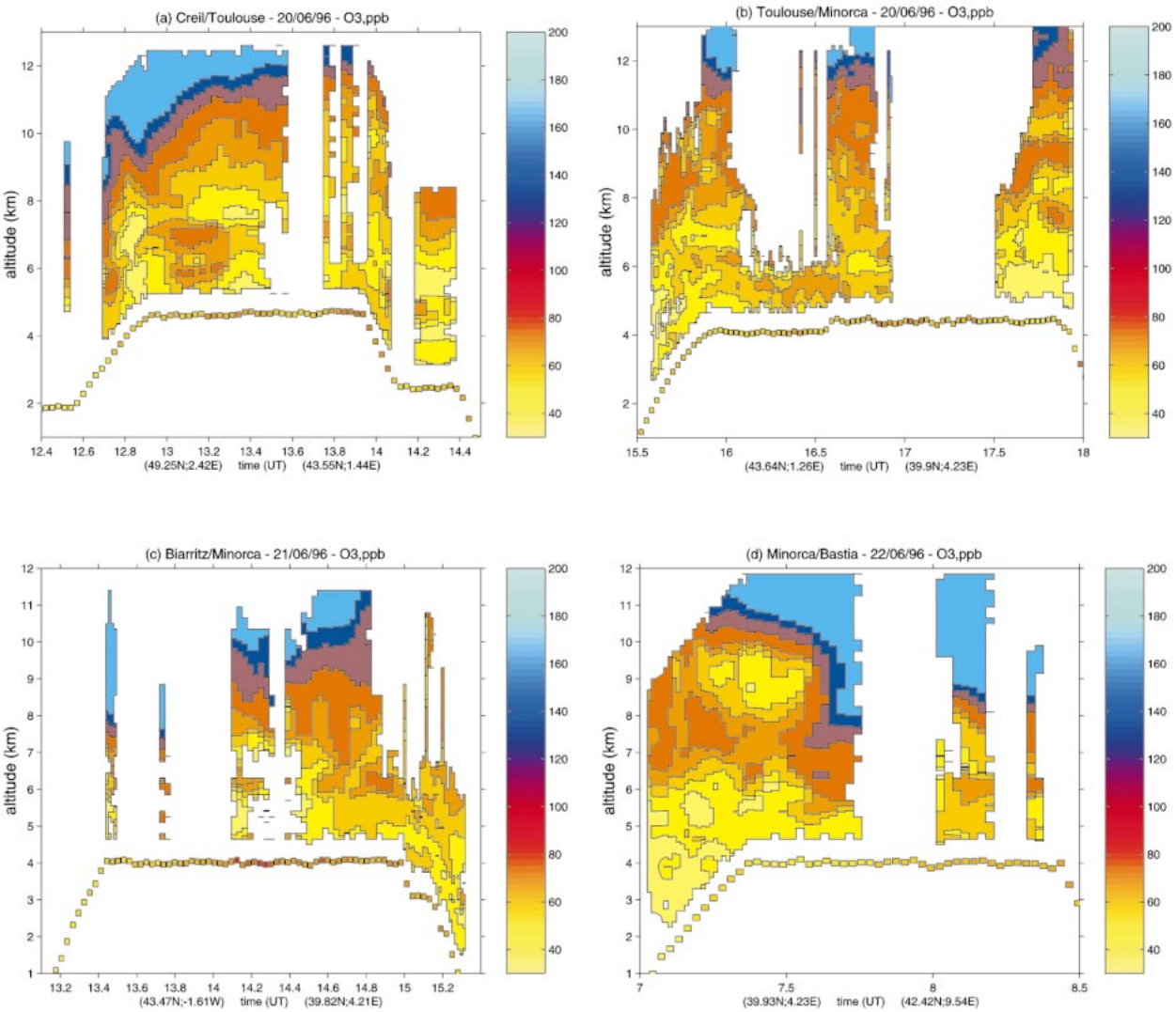

FIG. 4. The O_3 vertical profile time series measured by the airborne lidar for flights 6, 7, 9, and 10 (see Table 1). The geographical coordinates of takeoff and landing places are given in the label of the horizontal axis. The width of one pixel corresponds to a horizontal distance on the order of 10 km.

creases from 35 ppb down to 20 ppb (Roelofs and Lelieveld 1997). We will then assume that ozone gradient variation in the upper troposphere is mainly driven by dynamical mechanisms.

Several ozone layers observed in the frontal zone (Fig. 4) are correlated with the position of the jet streak maxima, identified in Fig. 3. This can be seen for the layers observed at 1300 UTC 20 June near 7 km, at 1412 UTC 21 June by the UV photometer, and at 0712 UTC 22 June near 7 km. It is then likely that the observed structures are related to tropopause folding processes followed by a strong differential advection in the jet core region. In Fig. 4, tilting of the vertical ozone gradient is clearly visible on the cyclonic side of the jet when these ozone layers are observed. This supports the hypothesis of stratospheric origin for these layers. Three ozone layers—observed at 8 km, 1418 UTC and 5.5 km, 1630 UTC 20 June and at 6.5 km, 1506 UTC 21 June—are not clearly related to a subsidence of air masses below the jet streak. But these ozone layers are below bands of high-altitude clouds observed in the lidar cross section (absence of data in Fig. 12) and in Meteosat pictures. It is difficult to conclude much about the connection between both observations although it is quite possible that dynamical mechanisms responsible for the cloud structure are also responsible for ozone layer formation. Bands of high-altitude clouds are related to patterns of the vertical velocity field formed by superposition of synoptic-scale events and mesoscale motions. This was documented during the First International Satellite Cloud Climatology Project (ISCCP) Regional Experiment field campaign held in 1986 (Starr and Wylie 1990). The origin of these layers will not be discussed further in this paper since this requires a de-

tailed analysis of dynamical processes using a 3D-mesoscale model, which will be done in future work.

b. Comparison with ECMWF analysis

Here, the altitude of the large ozone gradient between 80 and 200 ppb is used as a good diagnostic parameter to monitor tropopause horizontal variability. Indeed Bethan et al. (1996) have already shown that the tropopause can be defined in terms of the ozone mixing ratio. The ozone region 80–200 ppb corresponds to a 1.6–4 PVU potential vorticity range using an ozone-to-PV ratio characteristic of the lower stratosphere (50 ppb PVU^{-1}) (Beekmann et al. 1994). Comparisons of ozone and potential vorticity are then based on the 335- and 325-K isentropic horizontal distributions of the PV band 1.5–4 PVU, which have been calculated using ECMWF analysis (Fig. 5). Tropopause horizontal variability, characterized by ozone lidar cross sections in Fig. 4 at 10–11-km altitude on 20 June and at 8–9-km altitude on 21–22 June, is in good agreement with the PV map derived from ECMWF analysis. For this event, this shows that the meteorological analysis captures most of the dynamical structure modulating the tropopause at scales larger than 100 km (Fig. 5). Even the 80-ppb ozone maximum at 8 km is reproduced on 22 June by PV values larger than 1 PVU on the western edge of the COL. On the top of this layer, the 50-ppb ozone minimum at 9 km does not correspond (not shown) to lower PV values owing to the poor vertical resolution of the analysis near 300 hPa.

In addition to lidar data, other ozone measurements are available on 21 June from balloon soundings and from the measurement of ozone and water vapour by Airbus in-service aircraft (MOZAIC) database (Marenco et al. 1998). On 20 June, a MOZAIC aircraft flew from Paris to South America crossing the COL near 335 K above Spain between 1000 and 1112 UTC (Fig. 6). The flight track is perpendicular to the PV contours near the western edge of the PV anomaly while it remains close to the 3–4-PVU band on the eastern edge (Fig. 7). This explains the large difference of ozone time variation for both sides of the anomaly (Fig. 5). The sharp horizontal ozone gradient at 1118 UTC is consistent with a tilting of the tropopause on the western edge as observed by the lidar cross section on the next day. For the flight part close to the 3-PVU contour ozone modulation between 0930 and 1030 UTC is in good agreement with the oscillation of the PV contour on the isentropic surface.

On the same day, four ozonesondes were launched in different sites along the edge of the PV anomaly: Madrid (40.3°N, 3.4°W), Toulouse (43.6°N, 1.4°E), Gap (44.4°N, 6.0°E), and Payerne (46.8°N, 7.0°E). The Madrid, Toulouse, and Payerne soundings were made near 1200 UTC and ozone data are representative of the PV = 3 PVU region at 335 K (Fig. 6) and PV = 0.75 PVU at 315 K (Fig. 1). An ozone increase at 315 K for the

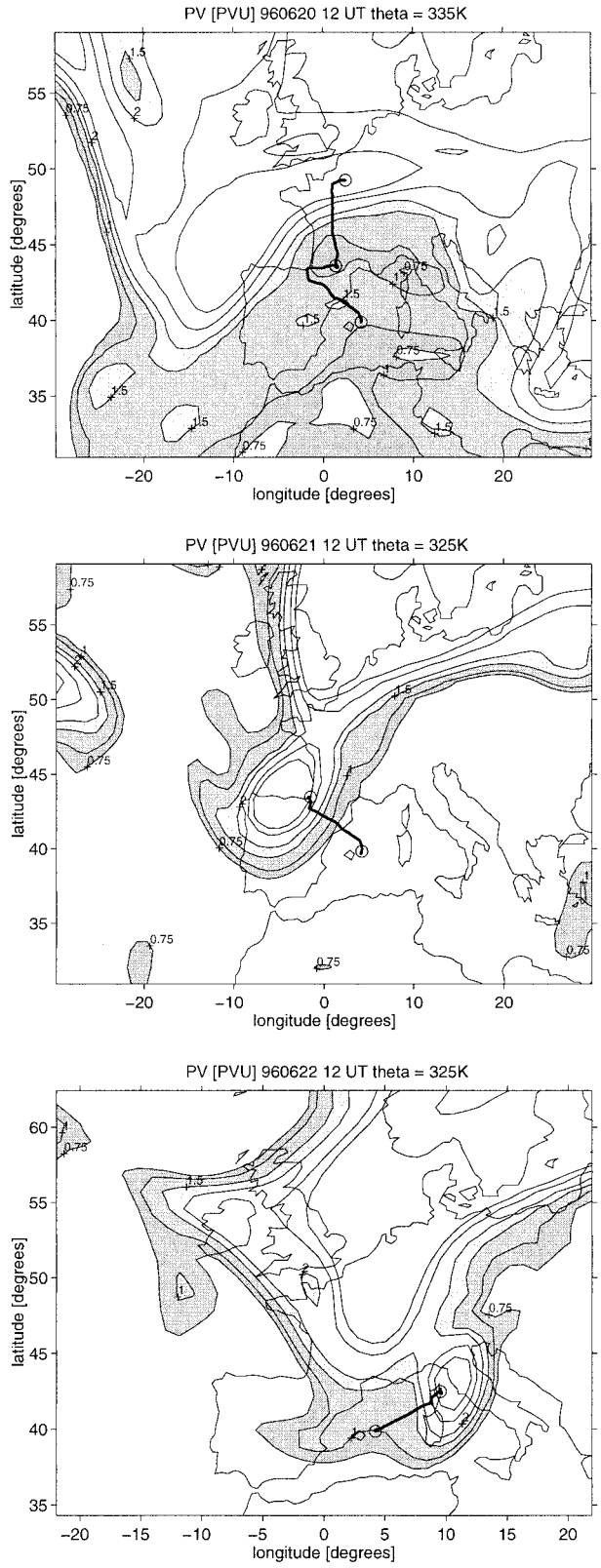

FIG. 5. (top) PV maps at 335 K at 1200 UTC 20 Jun and (middle), (bottom) at 325 K at 1200 UTC 21 and 22 Jun. PV contours are at 0.75, 1, 1.5, 2, 3, 4 PVU (PV < 0.75 PVU or PV > 2 PVU is white).

+3,6!0/3!1-,5/.8(473!4,./. !"#"! $%##&)+*

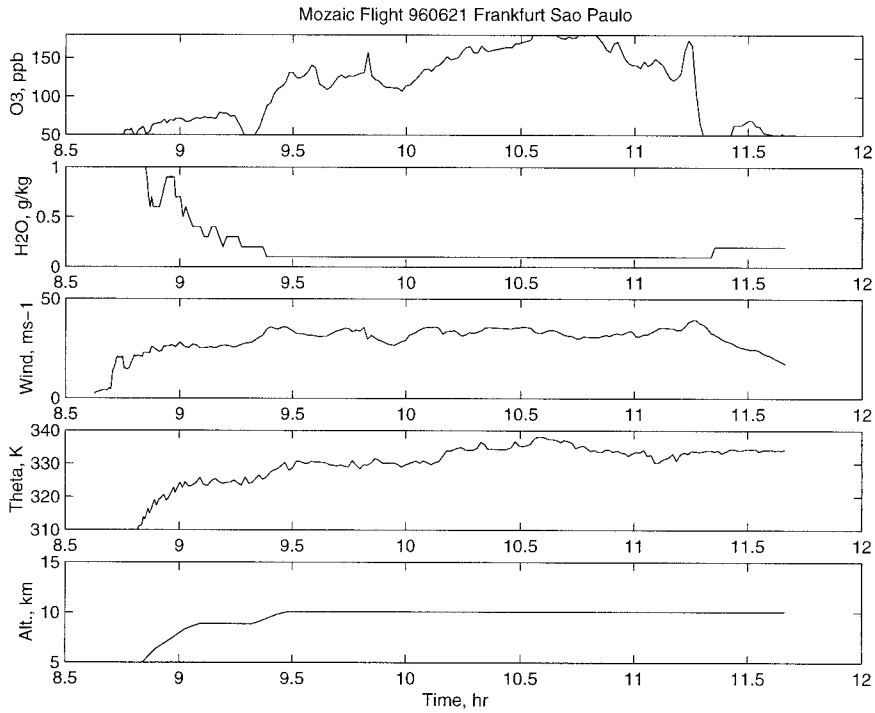

FIG. 6. Time series of the O_3, H_2O mixing ratios, wind speed, and potential temperature measured by the MOZAIC aircraft flying from Frankfurt to Sao Paulo on 21 Jun. (bottom) The aircraft's altitude is plotted.

Madrid and Toulouse soundings is consistent with the proximity of the PV anomaly (Fig. 8). The Gap sounding at 0930 UTC is less influenced by the COL with PV values less than 0.5 PVU at 315 K and less than 2 PVU at 335 K. The ozone profiles from the sondes are then in a good agreement with the PV distribution on the eastern edge of the COL. Furthermore, the Toulouse and Madrid ozone soundings are similar to ozone lidar profiles obtained near 1412 UTC during flight 9. Two ozone layers are indeed observed near 4.5 and 7.5 km in the sonde profiles and at 4 and 6 km in lidar data. Also the smooth positive vertical gradient between 8 and 11 km (i.e., between 320 and 335 K) appears in both datasets. This implies that the ozone lidar cross section perpendicular to the COL eastern edge is representative of a large fraction of the eastern edge of the PV anomaly. Combining the sondes and the lidar then gives a reliable estimate of the ozone field on the eastern side of the COL. To conclude this discussion on the good comparison between PV calculated from ECMWF analysis and the ozone variability near the tropopause, one can notice that the ozone to PV ratio for potential temperature larger than 320 K is close to the 50-ppb–PVU ratio characteristic of stratospheric air implying that strong diabatic processes associated with convective clouds did not perturb the ozone nor the PV distributions at these altitudes above 8 km.

c. *Analysis of the ozone gradient at the tropopause*

1) SIGNIFICANCE OF THE O_3 VERTICAL GRADIENT

In this section we will concentrate on the vertical ozone gradient evolution identified in the lidar cross section presented in Fig 4. The goal is to use the vertical ozone gradient $d\chi/dz$, where χ is the ozone mixing ratio and z the altitude, as a diagnostic tool to identify the influence of different transport mechanisms acting on ozone at the tropopause. This was already suggested by Price and Vaughan (1993) who have related transport mechanisms in COL to tropopause sharpness defined by radiosonde temperature profiles. In this paper we will add spatial dimension to this discussion using the horizontal variability of the tropopause sharpness derived from ozone lidar profiles. These profiles have been averaged over a time period where the ozone gradient appears to be stationary. This will remove part of the variations in ozone due to small-scale atmospheric variability. Before relating gradient to transport mechanisms, one must remember that the gradient $d\chi/dz$ remains sensitive to stretching of the isentropic surfaces since it can be written as the product of $d\chi/d\theta$ by $d\theta/dz$, where θ is potential temperature. A change in the stability of the atmosphere will thus modify the vertical ozone gradient $d\chi/dz$ and the total ozone column, as observed by McKenna et al. (1989) for ozone miniholes correlated with anticyclonic flows. But this does not

+3,6!0/3!1-,5/.8(4732 4,./. !"#"! $%##&)+*

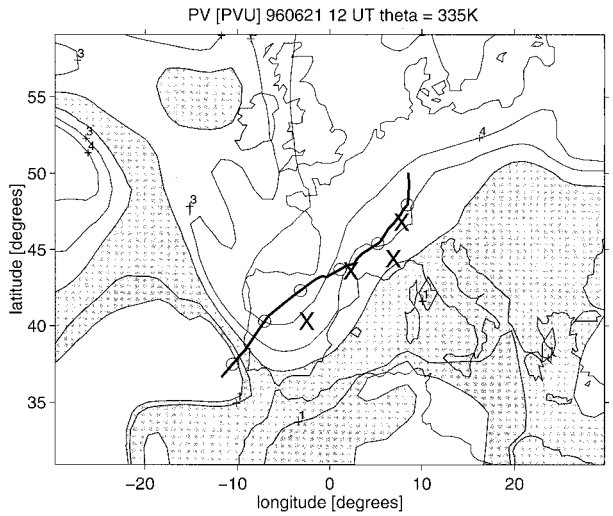

FIG. 7. MOZAIC aircraft trajectory plotted on the PV map at 335 K at 1200 UTC 21 Jun. PV contours are 0.75, 1, 2, 3, 4 PVU (PV < 0.75 PVU or PV > 3 PVU is white). The open circles represent the aircraft's position at 0900, 0930, 1000, 1030, 1100, and 1130 UTC (from right to left). The crosses represent the positions of the ozone sounding ground-based stations: Madrid, Toulouse, Gap, and Payerne (from south to north).

imply necessarily an ozone mixing between the stratosphere and the troposphere, which would lead to a change of $d\chi/d\theta$.

In the case of a positive PV anomaly, it has been shown (Hoskins et al. 1985; Thorpe 1986) that static stability is anomalously high in its center and that it is lower than the reference state in regions above and below the anomaly. Under the assumption of adiabatic motion, an air mass entering a region of the anomaly where the static stability is high will thus experience an increase of its vertical ozone gradient $d\chi/dz$, even if $d\chi/d\theta$ is conserved in this case. Therefore, before discussing the lidar dataset where one cannot calculate separately $d\chi/d\theta$ and $d\theta/dz$, it is first important to verify that the vertical stretching of the isentropic surfaces is not the dominant process in the ozone gradient variability observed for $d\chi/dz$ in the vicinity of the COL. Using a potential temperature vertical scale to plot the ozone soundings on 21 June (Fig. 7), one notices an increase of the positive gradient of the ozone mixing ratio between 320 and 330 K in Madrid, Payerne, and Toulouse, while this is not the case in Gap, where the ozone mixing ratio remains constant near 80 ppb. This implies that the stretching of the volume between the 320- and 330-K isentropic surfaces is not the unique factor responsible for smoothing of the mixing ratio vertical gradient $d\chi/dz$ observed on the edge of the anomaly. If this were the case, one should not observe a change in the mixing ratio gradient $d\chi/d\theta$ perpendicular to the isentropes at two different locations across the frontal zone. Therefore either vertical transport associated with convective clouds or differential advection of air masses near the tropopause, both being able to modify $d\chi/d\theta$, must play a significant role in the observed variability of the ozone gradient $d\chi/dz$ at the tropopause, at least at the eastern edge of the COL.

2) ANALYSIS OF THE LIDAR DATA

For flights 6, 7, and 9, each of the three ozone profile time series has been split into two subsets according to position from the COL center. The measurement times corresponding to this cut are, respectively, 1306, 1700, and 1400 UTC for these three flights. For flight 10, where different parts of the COL were sampled, the data were divided into three subsets: 0700–0734, 0739–0748, and 0800–0824 UTC. For this flight, profiles where the tropopause is strongly tilted have been removed from the average. Following the flight description in section 4a, nine different subsets can be sorted into five different air masses: frontal region west of the COL, western edge of the COL, the eastern edge of the COL, cloudy frontal area east of the COL, and a high pressure region far away from the COL. The latter one can be considered as a reference ozone profile against which one might compare the ozone distribution influence by atmospheric circulation near the COL.

The nine ozone profiles are shown in Fig. 9 including the straight line fit to the vertical profile for two concentration intervals: 80–120 ppb (upper troposphere) and 120–200 ppb (lowermost stratosphere). The 120-ppb threshold has already been viewed as a valid criteria for separating tropospheric and stratospheric air (Thouret et al. 1998). This corresponds to a 2.4-PVU dynamical tropopause, which is in good agreement with the 1.6–3 PVU range used to define the tropopause (Hoerling et al. 1993). Ozone is thus used to define the position of the air mass relative to the tropopause. As shown by Bethan et al. (1996), this is very useful in highly cyclonic regions where the thermal tropopause is very often indefinite. But those authors recommend an 80-ppb value to define the tropopause and to estimate the tropospheric ozone content. This lower limit is useful to define the top of the tropospheric column, but not necessarily to separate different dynamical processes in the tropopause region.

In Table 2, the values of the vertical gradient $d\chi/dz$ are given for the different air masses. For the reference state, one cannot distinguish between the ozone gradient in the troposphere and lower stratosphere. This means that the 120-ppb ozone threshold is not very well suited to define the barrier between tropospheric and stratospheric air in anticyclones. This is a good indication that mixing occurs in high pressure regions. It might be related to the weaker influence of the strong vertical differential advection bringing air from the polar front where a strong ozone gradient can be maintained. On the contrary, frontal regions are very likely to exhibit strong ozone vertical gradients, in good agreement with the suggestion of McIntyre and Palmer (1984) that syn-

+3,6:0/3:1-,5/.8(4732 4,./. !"#"! $%##&)+*

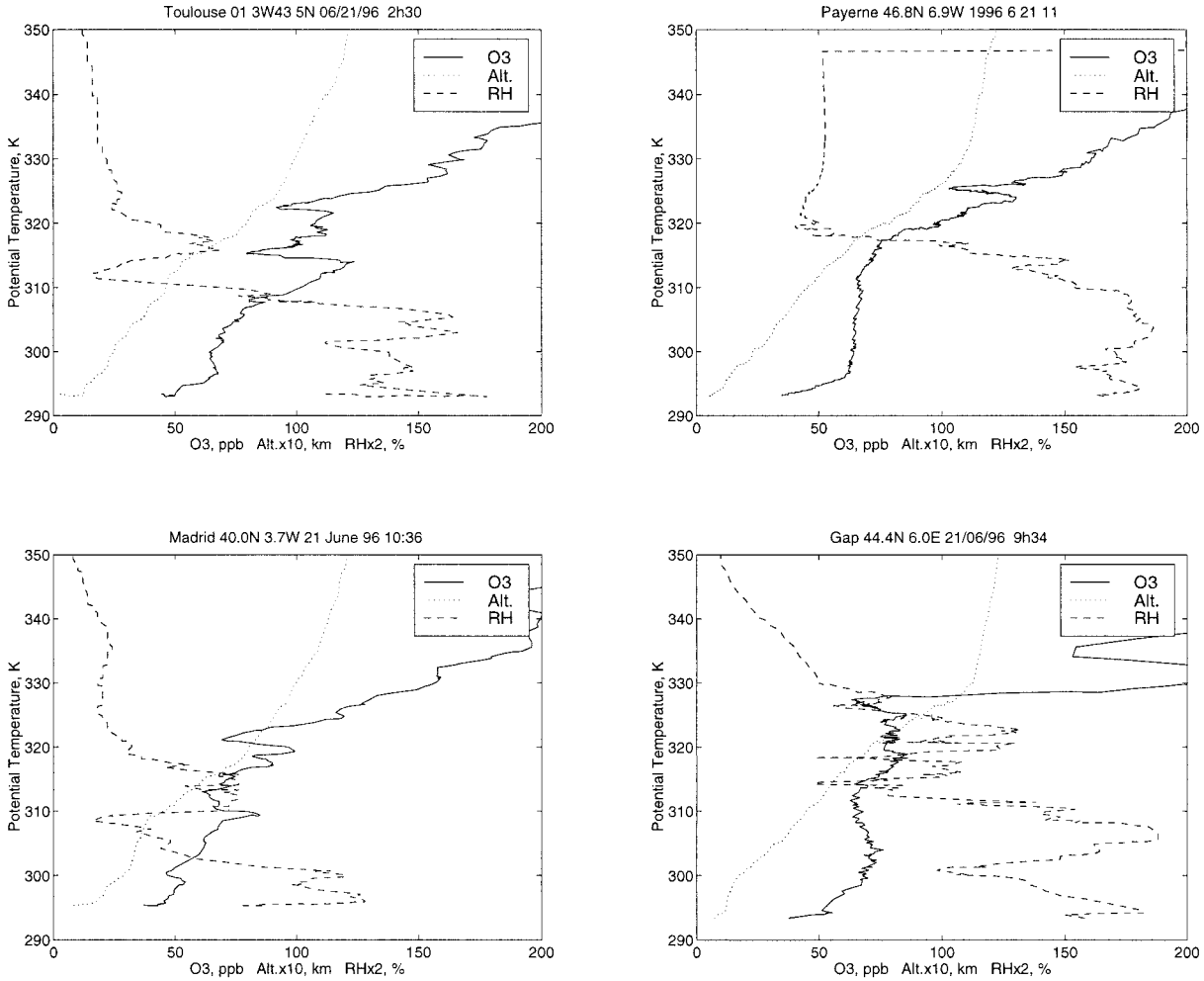

FIG. 8. The O_3 mixing ratio and relative humidity vs potential temperature as measured by ozone soundings performed in Toulouse, Payerne, Madrid, and Gap on 21 Jun.

optic-scale baroclinic eddies can sharpen the isentropic gradients of PV marking the extratropical tropopause.

Indeed, for the four regions around the COL, and contrary to the reference state, there is a clear separation of the upper-tropospheric part of the flow from the lowermost stratosphere where gradients are always stronger. The vertical differential advection encountered in its frontal zones must play a significant role to maintain this separation that must have arisen before the low cuts off from the general circulation. Accordingly, the tropospheric–stratospheric contrast decreases with time, as the jet streak at 250 hPa does between 20 and 21 June in the return flow associated with the eastern front (Fig. 3). However, strongest values of the vertical ozone gradient are found in the northerly flow associated with the western front, a region where on 22 June the jet streak is much weaker than on the eastern flank on 20–21 June (not shown here). But the COL is then under the influence of a larger trough. Observed gradients on this side may thus be more representative of the sharp gradient associated with the frontal zone of the general circulation than of the COL itself. Other mechanisms are likely to account for variability of the vertical ozone gradient in the frontal regions, especially when comparing the eastern side to the western one. Indeed, turbulent mixing is enhanced in the presence of the strong jet streak on the eastern side and will tend to smooth the sharp gradient induced by differential advection. This has been documented by several experimental studies using aircraft (Shapiro 1978) or clear air VHF radar data (Caccia and Cammas 1998). This may partly explain why smoother values of the vertical gradient are found on the eastern side. However, it must be a second-order mechanism compared to differential advection; otherwise, variation of the gradient in the eastern front regions should be opposite to the one observed. A striking difference is also that the atmosphere is cloudless in the western front area and cloudy in the eastern one, where isentropic motions are upwelling. However, it is not obvious to identify a transport mechanism related

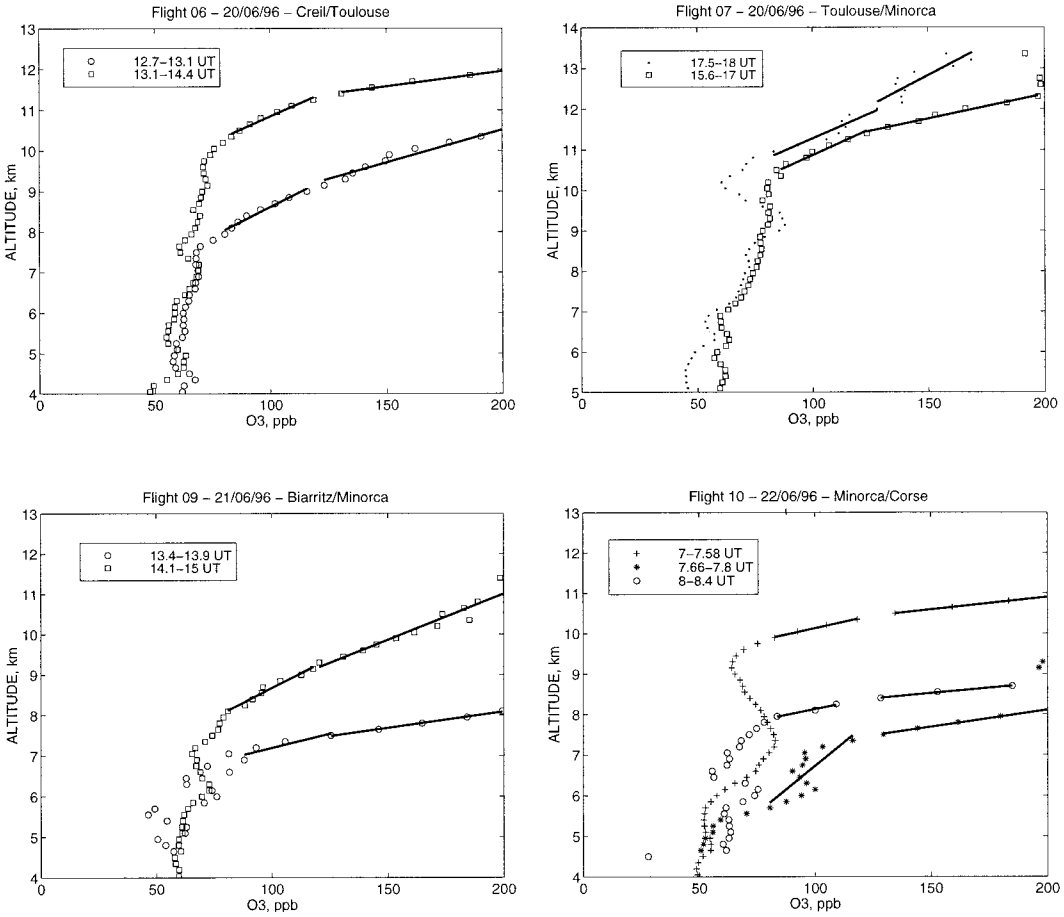

FIG. 9. Lidar ozone profiles averaged over the given time interval for flights 6, 7, 9, and 10. The heavy lines are linear fits to the profiles in the 80–120- and 120–200-ppb ozone ranges. Correspondence between the symbols and the air masses is given in Table 2.

to the cloud development and capable of smoothing the ozone and stability gradient at the tropopause.

The second noticeable feature in Table 2 is the weak tropospheric ozone vertical gradient within the COL when no convective clouds are present. The smallest values are observed in the upper troposphere at the edges of the COL. This is probably due to lower static stability usually observed in the troposphere below the center of the PV anomaly. Moreover, a larger turbulent mixing below the jet, where vertical wind shear is generally largest, may also account for these observations. At this stage, it is not possible to separate both mechanisms. Finally, the ozone gradient at the eastern edge of the COL varies significantly whether convective clouds have developed below the COL or not. Both in the upper troposphere and the lowermost stratosphere, it increases strongly once the PV anomaly has been convectively eroded. Indeed, this erosion will sharpen the ozone gradient at the tropopause, accounting for the large values observed in the upper troposphere. Convection will also mix stratospheric air into the troposphere, which leads to an increase of the ozone background level (cf. section 5). For the lowermost stratosphere using the vertical ozone gradient it is not possible to distinguish enhancement of the gradient induced by convection from the gain of static stability still to be found within the remaining PV anomaly.

5. Decay of the second COL on 25–26 June

a. Description of the flights in the second COL

From 25 to 26 June, four aircraft flights were carried out in the new COL located over the Genova Gulf (Table 1). The rationales for these new flights in a different COL system were twofold: 1) the new COL builds up from the trough that absorbed the first COL, and 2) the new COL decays without further interaction with the polar front. Therefore one may expect to sample air being influenced by the first COL, and transport of stratospheric air to the troposphere may be more effective for this COL, which breaks up without returning to the polar reservoir. From the aircraft trajectories shown in Fig. 1, one can notice that, contrary to the

+3,650/351-,5/.8(47324,./. !"#"! $%##&)+*

TABLE 2. Ozone vertical gradients (ppb km^{-1}) and corresponding flight numbers for two ozone ranges in different air masses around the COL: high pressure (HP), western front (WF), western COL edge (WE), eastern COL edge (EE), and eastern front (EF).

Ozone range (ppb)	HP(●)	WF (+)	WE (*)	EE (○)	EF (□)
80–120	41 (F7)	80 (F10)	22 (F10)	35 (F6)	40 (F6)
				72 (F9)[a]	39 (F7)
				88 (F10)[a]	35 (F9)
120–200	33 (F7)	162 (F10)	119 (F10)	62 (F6)	134 (F6)
				124 (F9)[a]	83 (F7)
				189 (F10)[a]	44 (F9)

[a] Influence of convective clouds.

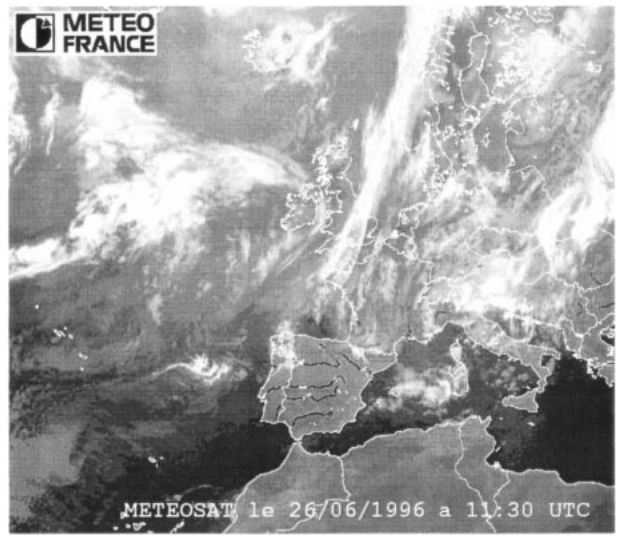

FIG. 10. Meteosat satellite IR image at 1130 UTC 26 Jun 1996.

previous period, most data are collected in the northerly flow around the COL. For the two flights near Corsica, the COL was crossed near a wedge of low potential vorticity at 315 K. This region corresponds also to upper-level clouds seen in the Meteosat IR picture for 1130 UTC 26 June (Fig. 10). It implies that a streamer of humid tropospheric air penetrated the positive PV anomaly on its western flank.

b. Discussion of the ozone dataset

The ozone vertical cross sections through this second COL are presented in Fig. 11 using the same color scale as for Fig. 4 for the ozone mixing ratio contour lines. As expected with air masses sinking from the upper troposphere, cloudiness on the western flank of the COL was not a problem for these four flights. Again one can notice the good agreement between the lidar cross section and the in situ measurements of the aircraft. In both cases the largest ozone values, recorded in the 4–5-km altitude band, are obtained below the COL during the flights arriving to and departing from Figari in Corsica.

The most striking feature in Fig. 11 as compared to Fig. 4 is the ozone values in the midtroposphere below the PV anomaly are larger for the second COL (>70 ppb) than for the first one (<60 ppb). This is especially true for the ozone in situ aircraft measurements near 4 km. To identify a correlation between this ozone enrichment of the midtroposphere and the decay of the first COL system, two clusters of airmass back kinematic trajectories were calculated using ECMWF analyses. These trajectories end, respectively, at 400 hPa on 1400 UTC 25 June, and 1000 UTC 26 June, in the ozone-rich region observed below the COL (Fig. 12). Markers on the figures indicate the air mass position at their arrival and three days (Fig. 12a) or four days (Fig. 12b) before. Some air masses came from the polar reservoir and remained almost isobaric. They may have been rich in ozone since then. But several trajectories moved through the area above the Genova Gulf on 21–22 June. We have seen before that this is a region where convection may play a significant role on the eastern side of the COL. Indeed, these air masses experience strong upward motions at that time (lower panel of Figs. 12a and 12b). This may lead to their ozone enrichment through mixing with lower-stratospheric air masses. However, it is not possible to rule out those air masses were already rich in ozone since they came from the boundary layer.

In addition to ozone enrichment of the midtroposphere, well-developed tropopause folds on the western side and local ozone minima below the COL are observed in the lidar cross sections. The tropopause fold seen during the last flight between Vichy and Creil is in surprisingly good agreement with the PV streamer shown on the 315-K isentropic surface considering the poor resolution of the analysis (T-106). The large ozone–PV ratio in this layer (100 ppb–PvU) is probably related to underestimate of PV in the streamer (Ancellet et al. 1991). But Lamarque and Hess (1994) showed that PV tendency is negative in a tropopause fold and depends both on the effect of diffusion on wind and on temperature. As ozone turbulent mixing is not necessarily proportional to PV diffusion, part of the large ozone–PV ratio may also point to turbulent mixing modifying PV in the fold. The ozone local minima observed at 1030 UTC 26 June, on the top of a 100-ppb ozone peak at 6 km, is well correlated with two ozone profiles performed on the same day in Gap by an electrochemical sonde and in Frankfurt (50.04°N, 8.56°E) by a MOZAIC aircraft (Fig. 13). This means that the ozone-rich layer at 6 km remained well separated from the tropopause region over a significant horizontal distance (1000 km) along the frontal region. The cloud distribution revealed by the IR Meteosat image shows the same thing, namely a long band of high-altitude clouds along the eastern border of France on 26 June (Fig. 10). Such interleaving of low and high ozone layers at tropospheric level is likely to stimulate irreversible mixing of tropospheric and stratospheric air.

+3,6!0/3!1-,!/.8(473!4,./. !"#"! $%##&)+*

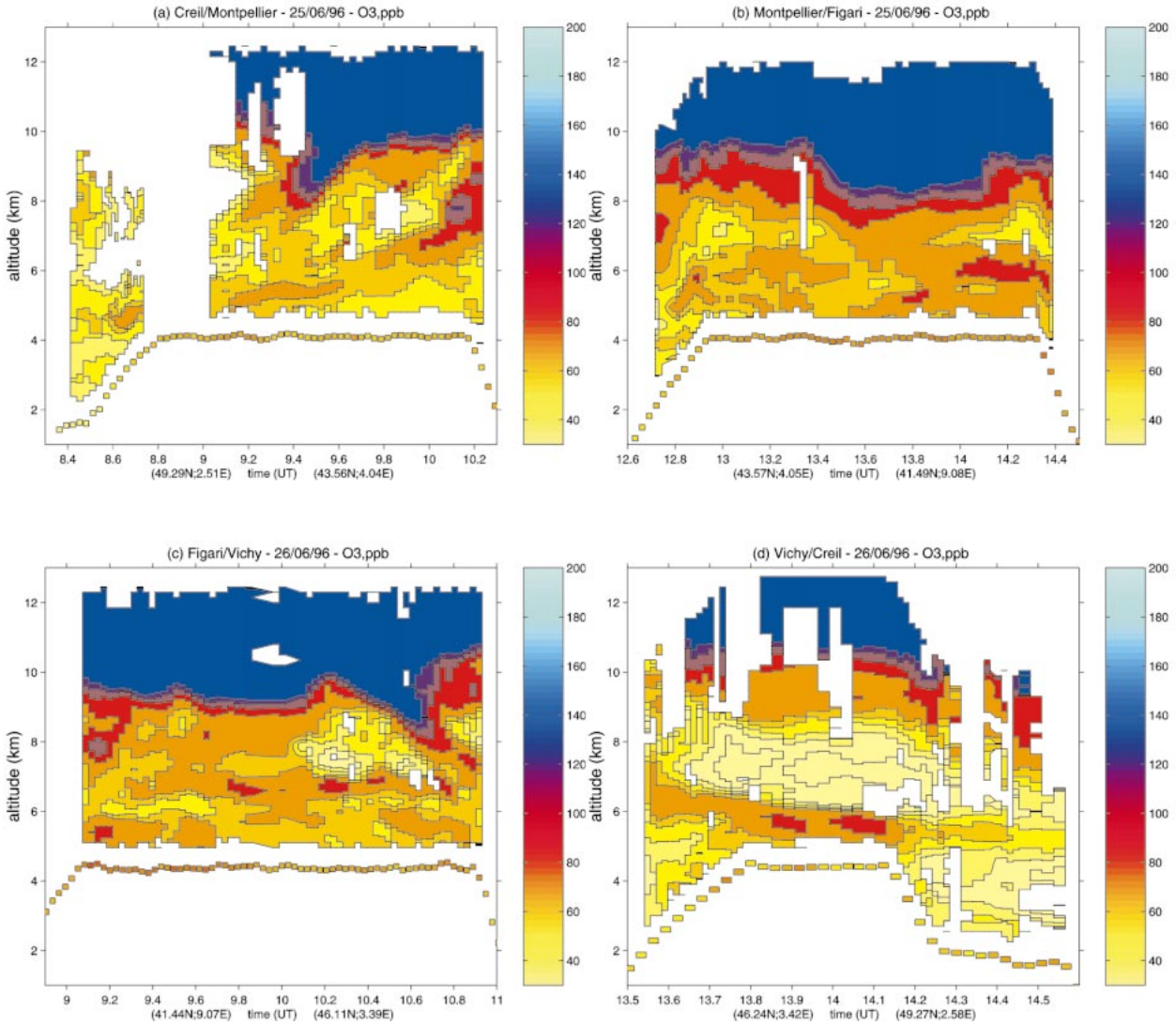

FIG. 11. The O_3 vertical profile time series measured by the airborne lidar for flights 13, 14, 15, and 16 (see Table 1). The geographical coordinates of takeoff and landing places are given in the label of the horizontal axis. The width of one pixel corresponds to a horizontal distance on the order of 10 km.

6. Conclusions

From several ozone vertical cross sections measured with an airborne lidar, we documented the decaying phase of a cutoff low with a high spatial resolution. The description of temporal evolution of this COL was not easy to explain as it merged into a larger trough. But it was possible to get useful data in various areas in and around the COL, especially on its eastern side, which is usually difficult from the ground. Comparing well with complementary data, these cross sections turn out to give a realistic description of the ozone field. Two main features are observed: a large variability of the ozone vertical gradient at the tropopause and numerous ozone-rich layers in the midtroposphere.

The first feature is to be linked with a splitting induced by the COL between the upper troposphere and lowermost stratosphere. A change in vertical stability, increasing in the stratospheric part of the PV anomaly but decreasing below, modifies the vertical ozone gradient but it cannot account for all its observed variability. Other dynamical processes account for it. Differential advection in frontal regions and convection, when taking place, tend to sharpen this gradient. On the contrary, turbulent mixing in the presence of a strong jet streak tends to smooth it.

There is also a very clear differentiation between the western and eastern part of the COL. First, air masses in the return flow on the eastern side are upwelling, which favors the formation of convective clouds and of narrow bands of cirrus clouds. Second, the jet streak associated with this cyclonic flow is larger on the eastern side. Contrary to the first one, the latter observation is

+3,650/351-,5/.8(4734,./. !"#"! $%##&)+*

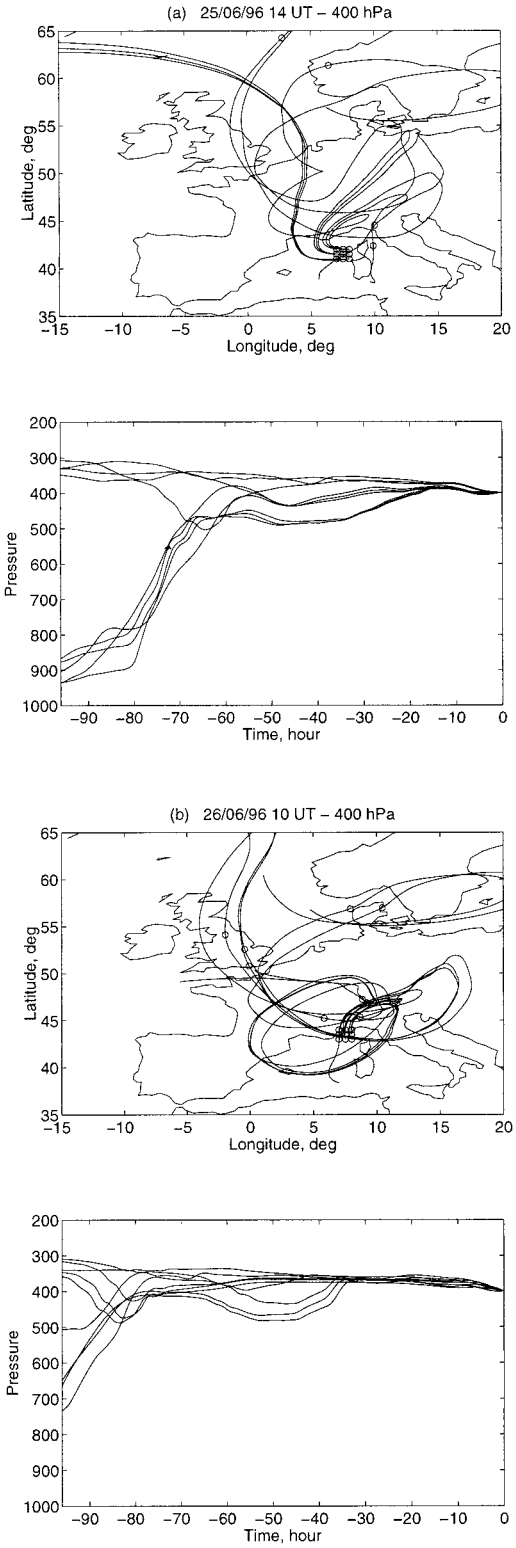

FIG. 12. (a) 3D back trajectories ending at 1400 UTC 25 Jun at 400 hPa between 41°N, 7°E and 42°N, 8°E. (b) 3D back trajectories ending at 1000 UTC 26 Jun at 400 hPa between 43°N, 7°E and 44°N, 8°E.

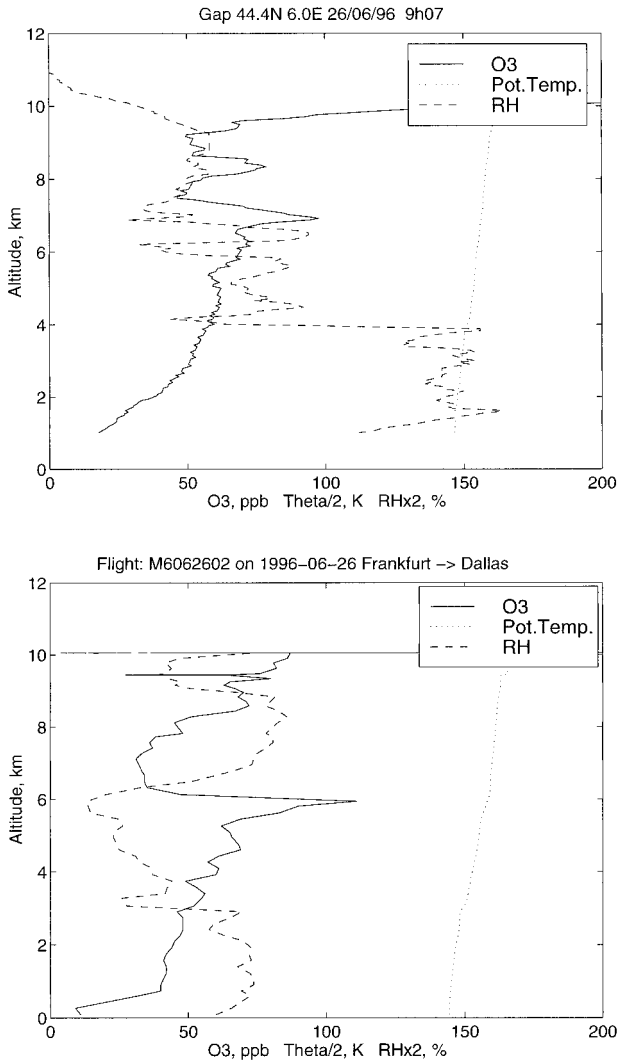

FIG. 13. The O_3 and relative humidity vertical profiles measured on 26 Jun (top) by an ozonesonde launched in Gap at 0900 UTC and (bottom) by a MOZAIC aircraft during its ascent over Frankfurt at 0830 UTC.

highly unlikely to be a generic characteristic of a COL. Indeed, the weak jet streak observed on the western side may result from the interaction of this COL with a larger trough.

The transport of ozone from the stratosphere to the troposphere was not addressed here. However, convective erosion of the COL, tropopause folding on the side of the COL, and clear air turbulence in the vicinity of the jet streak should play a significant role. Indeed, such mechanisms were observed here and the background ozone level increased with time below the COL.

The second feature was not studied in detail here, but the presence of numerous thin ozone-rich layers tends to reinforce the idea that layering is an intrinsic property of the troposphere (Newell et al. 1996). For this case study, their stratospheric origin was not always estab-

lished. However, a link sometimes observed with the stratospheric reservoir and the high ozone in their core tend to discard the idea of a photochemical origin. Being trapped in the free troposphere, they contribute to the budget of tropospheric ozone. The magnitude of this contribution remains an open question at this stage.

Acknowledgments. This work has been supported by the CEC-DG-12 under the TOASTEC program. The ALTO lidar system development was supported by CNRS/INSU, ADEME, and the Ministre de la Recherche. The Service d'Aronomie and INSU/DT technical staff are gratefully acknowledged for their support. The ECMWF center is acknowledged for providing the meteorological analysis. The Spanish Instituto Nacional de Meteorologia, Météo-France, CNES, and the Swiss meteorological office are acknowledged for making the ECC soundings, in Madrid, Toulouse, Gap, and Payerne, respectively.

REFERENCES

Ancellet, G., and F. Ravetta, 1998: Compact airborne lidar for tropospheric ozone: Description and field measurements. *Appl. Opt.,* **37,** 5509–5521.

——, J. Pelon, M. Beekmann, A. Papayannis, and G. Megie, 1991: Ground-based lidar studies of ozone exchanges between the stratosphere and the troposphere. *J. Geophys. Res.,* **96,** 401–421.

——, M. Beekmann, and A. Papayannis, 1994: Impact of a cut-off low development on downward transport of ozone in the troposphere. *J. Geophys. Res.,* **99,** 3451–3468.

Appenzeller, C., and H. C. Davies, 1992: Structure of stratospheric intrusions into the troposphere. *Nature,* **358,** 570–572.

——, ——, and W. A. Norton, 1996: Fragmentation of stratospheric intrusions. *J. Geophys. Res.,* **101,** 1435–1456.

Bamber, D. J., P. G. W. Healey, B. M. R. Jones, S. A. Penkett, A. F. Tuck, and G. Vaughan, 1984: Vertical profiles of tropospheric gases: Chemical consequences of stratospheric intrusions. *Atmos. Environ.,* **18,** 1759–1766.

Beekmann, M., G. Ancellet, and G. Megie, 1994: Climatology of tropospheric ozone in southern Europe and its relation to potential vorticity. *J. Geophys. Res.,* **99,** 12 841–12 853.

Bethan, S., G. Vaughan, and S. J. Reid, 1996: A comparison of ozone and thermal tropopause heights and the impact of tropopause definition on quantifying the ozone content of the troposphere. *Quart. J. Roy. Meteor. Soc.,* **122,** 929–944.

——, ——, C. Gerbig, A. Volz-Thomas, H. Richer, and D. Tiddeman, 1998: Chemical air mass differences near fronts. *J. Geophys. Res.,* **103,** 13 413–13 434.

Browell, E. V., S. Ismail, and S. T. Shipley, 1985: Ultraviolet DIAL measurements of 0_3 profiles in regions of spatially inhomogeneous aerosols. *Appl. Opt.,* **24,** 2827–2836.

Caccia, J.-L., and J.-P. Cammas, 1998: VHF-ST radar observations of an upper-level front using vertical and oblique-beam C_N^2 measurements. *Mon. Wea. Rev.,* **126,** 483–501.

Chedin, A., N. A. Scott, C. Wahiche, and P. Moulinier, 1985: The improved initialization inversion method: A high resolution physical method for temperature retrievals from satellites of the TIROS-N series. *J. Climate Appl. Meteor.,* **24,** 128–143.

Hoerling, M. P., T. K. Schaack, and A. J. Lenzen, 1993: A global analysis of stratospheric–troposheric exchange during northern winter. *Mon. Wea. Rev.,* **121,** 162–172.

Holton, J. R., P. H. Haynes, M. E. McIntyre, A. R. Douglass, R. B. Rood, and L. Pfister, 1995: Stratosphere–troposphere exchange. *Rev. Geophys.,* **33,** 403–439.

Hoskins, B. J., M. E. McIntyre, and A. W. Robertson, 1985: On the use and significance of isentropic potential vorticity maps. *Quart. J. Roy. Meteor. Soc.,* **111,** 877–946.

Kley, D., J. Beck, P. Greenfelt, O. Hov, and S. A. Penkett, 1997: Tropospheric Ozone Research (TOR): A sub-project of EUROTRAC. *J. Atmos. Chem.,* **28,** 1–9.

Lamarque, J.-F., and P. G. Hess, 1994: Cross-tropopause mass exchange and potential vorticity budget in a simulated tropopause folding. *J. Atmos. Sci.,* **51,** 2246–2269.

Langford, A. O., and S. J. Reid, 1998: Dissipation and mixing of a small-scale stratospheric intrusion in the upper troposphere. *J. Geophys. Res.,* **103,** 31 265–31 276.

——, C. D. Masters, M. H. Proffitt, E.-Y. Hsie, and A. F. Tuck, 1996: Ozone measurements in a tropopause fold associated with a cut-off low system. *Geophys. Res. Lett.,* **23,** 2501–2504.

Marenco, A., and Coauthors, 1998: Measurement of ozone and water vapor by Airbus in-service Aircraft: The MOZAIC airborne program, an overview. *J. Geophys. Res.,* **103,** 25 631–25 642.

McIntyre, M. E., and T. N. Palmer, 1984: The ''surf zone'' in the stratosphere. *J. Atmos. Terr. Phys.,* **46,** 825–849.

McKenna, D. S., R. L. Jones, J. Austin, E. V. Browell, M. P. McCormick, A. J. Krueger, and A. F. Tuck, 1989: Diagnostic studies of the Antarctic vortex during the 1987 Airborne Antarctic Ozone Experiment: Ozone miniholes. *J. Geophys. Res.,* **94,** 11 641–11 668.

Molina, L., and M. Molina, 1986: Absolute absorption cross section of ozone in the 185 to 350 nm wavelength range. *J. Geophys. Res.,* **91,** 14 501–14 508.

Newell, R. E., and Coauthors, 1996: Vertical fine-scale atmospheric structure measured from NASA DC-8 during PEM-West A. *J. Geophys. Res.,* **101,** 1943–1960.

Price, J. D., and G. Vaughan, 1993: The potential for stratosphere–troposphere exchange in cut-off low systems. *Quart. J. Roy. Meteor. Soc.,* **119,** 343–365.

Roelofs, G.-J., and J. Lelieveld, 1997: Model study of the influence of cross-tropopause O_3 transports on tropospheric O_3 levels. *Tellus,* **49B,** 38–55.

Shapiro, M. A., 1978: Further evidence of the mesoscale and turbulent structure of upper level jet stream-frontal zone systems. *Mon. Wea. Rev.,* **106,** 1100–1111.

Starr, D. O'C., and D. Wylie, 1990: The 27–28 October 1986 FIRE cirrus case study: Meteorology and clouds. *Mon. Wea. Rev.,* **118,** 2259–2287.

Thorpe, A. J., 1986: Synoptic scale disturbances with circular symmetry. *Mon. Wea. Rev.,* **114,** 1384–1389.

Thouret, V., A. Marenco, P. Nedelec, and C. Grouhel, 1998: Ozone climatology at 9–12 km altitude as seen by the MOZAIC airborne program between September 1994 and August 1996. *J. Geophys. Res.,* **103,** 25 653–25 680.

Wirth, V., 1995: Diabatic heating in an axisymmetric cut-off cyclone and related stratosphere–troposphere exchange. *Quart. J. Roy. Meteor. Soc.,* **121,** 127–147.

+3,6!0/3!1-,5/.8(473!4,./. !"#"! $%##&)+*